C. H. LEE
Graduate Student.

SHIRO KOBAYASHI
Professor of Mechanical Engineering.

Mechanical Design, University of California, Berkeley, Calif.

Analyses of Axisymmetric Upsetting and Plane-Strain Side-Pressing of Solid Cylinders by the Finite Element Method

Detailed studies of the deformation characteristics in axisymmetric upsetting and plane-strain side-pressing were attempted by the finite element method. Solutions were obtained up to a 33 percent reduction in height in axisymmetric upsetting and up to a 19 percent reduction in height in side-pressing, under conditions of complete sticking at the tool-workpiece interface. Load-displacement curves, plastic zone development, and strain and stress distributions were presented, and some of the computed solutions were compared with those found experimentally.

Introduction

An important problem involved in predicting defects occurrence in plastic deformation processes is the accurate determination of local states of stress and strain in the deforming material. In many forging operations, the geometrical configuration of a deforming body continuously changes during the process. The body may contain an elastic region as well as a plastic region, and one region may experience unloading while another undergoes continued loading. In developing a theory for finding complete solutions to problems of this type, these aspects must be taken into consideration. The present investigation concerns two problems in this category: the axisymmetric upsetting and the plane-strain side-pressing of solid cylinders.

When an elastic-plastic material is continuously loaded from a stress-free state, the plastic and elastic components of the strain are at first comparable. As the loads are increased, the plastic zone expands to a size where the constraint due to the elastic region becomes locally ineffective. Large strains are then possible, and the overall distortion increases at a rate controlled by the changing shape of the specimen. Our primary interest is with this range of unrestricted plastic flow. To determine the changing shape of the specimen in unrestricted flow it is necessary to follow the path of deformation. Therefore, the finite element method is used in this study.

The finite element formulation [1][1] was developed originally for structural analysis and it has been used for solving many complex structural problems. In the area of nonlinear problems, particularly those of plasticity, only a few solutions are now available for problems of contained plastic flow. It is possible to extend the method to problems of unrestricted plastic flow, although questions with regard to the accuracy of the solution and the efficiency of the computation will undoubtedly arise.

In axisymmetric upsetting, the cylindrical free surface barrels when friction exists at the interface, and fracture occurs at the barreled surface. An analytical treatment of the problem of free surface barreling has been attempted by several investigators. Hill [2] proposed a general method of analysis for metal-working processes with which it was possible to analyze the incipient barreling. Tarnovskii, et al. [3] assumed a form for radial displacement which contained the parameters characterizing inhomogeneous deformation. The parameters were determined by the variational method, neglecting the effect of the axial displacement distribution. Although the theoretical predictions for barreling found by these methods compared well with experimental results for small deformations, no complete theoretical solution has yet been suggested for the entire process of upsetting.

The slip-line theory has been well developed for the analysis of plane-strain problems. The slip-line solutions of indentation and compression for rigid perfectly plastic materials [4, 5, 6] can be utilized for an analysis of the plane-strain side-pressing of cylinders. However, the effects of elastic behavior and work-hardening on the yield point load of real materials are not known, and a detailed solution for the deformation that takes place during continued loading beyond the yield point is lacking.

Contributed by the Production Engineering Division and presented at the Winter Annual Meeting, New York, N. Y., November 29–December 3, 1970, of The American Society of Mechanical Engineers. Manuscript received at ASME Headquarters, July 23, 1970. Paper No. 70-WA/Prod-4.

[1] Numbers in brackets designate References at end of paper.

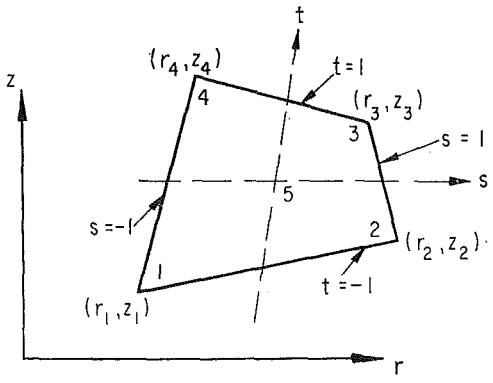

Fig. 1 Quadrilateral element and natural coordinate system

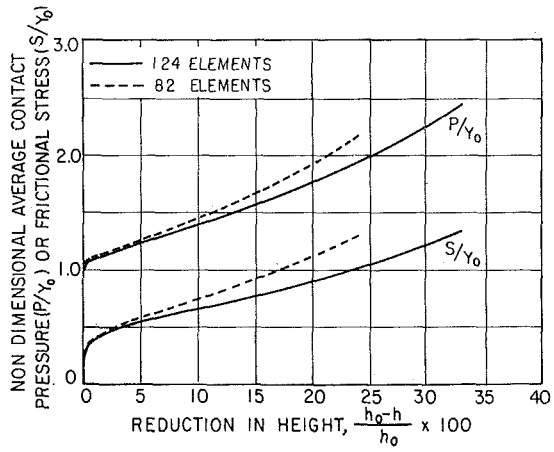

Fig. 2 Average contact pressure and frictional stress as functions of reduction in height

In this paper, using an improved finite element representation, a detailed study of the deformation characteristics was attempted for axisymmetric upsetting and plane-strain side-pressing of solid cylinders under conditions of complete sticking at the tool-workpiece interface.

Method of Analysis

A variational formulation of elastic-plastic behavior of materials in the absence of body forces assumes a stationary value of the functional

$$\Phi = \frac{1}{2}\int_V (\dot{\sigma}^T\dot{\varepsilon})dV - \int_S (\dot{U}^T\dot{F})dS \qquad (1)$$

where $\dot{\sigma}$ is the stress-rate vector; $\dot{\varepsilon}$, the strain-rate vector; $\dot{U}$, the velocity vector; and $\dot{F}$, the distribution of the given external stress-rate vector. The superscript T denotes the transpose. The distribution of the stress-rate vector, $\dot{\sigma}$, is associated with the strain-rate vector, $\dot{\varepsilon}$, which is derivable from a continuous velocity vector, $\dot{U}$, differing infinitesimally from the actual distribution, and satisfying the boundary conditions. The surface integral of the second term in equation (1), while the first integral is taken through the volume of mass, exists only over the part of the surface which is subjected to the stress-rate, $\dot{F}$.

A continuum of elastic-plastic body is divided into elements interconnected at a finite number of nodal points. The functional is then approximated by a function of nodal point values. In the displacement method, these nodal point values are the displacement (or velocity) components.

The discretization of the variational problem is performed on the elemental level by approximating the functional with respect to the mth element by a function of the mth element nodal point values. This approximation is accomplished by replacing the actual distribution with an approximating velocity distribution in each element. When an appropriate operator is applied to the approximated velocities, the strain-rate components in the element are derivable and the stress-rate components can be expressed in terms of strain-rate components. For isotropic materials the stress-rate and strain-rate components are associated by Hooke's law in the elastic region and by the Prandtl-Reuss equations during continued loading in the plastic region. The functional (1), summing the functionals of subregions, is then approximated by the function of nodal point variables. Applying the variational principle to this approximating function results in the simultaneous equations for the unknown velocity components at the nodes of the region, in the form

$$\dot{R} \approx K\dot{u} \qquad (2)$$

where $\dot{u}$ is the nodal point velocity vector, K is the stiffness matrix, and $\dot{R}$ is the equivalent nodal point force-rate vector. The solution of the simultaneous equations for the nodal point velocities and the elemental distributions then provide the approximate solution to the actual velocity distribution.

When we consider mixed boundary conditions where the velocity vectors over a part of the surface are described, the matrix equation for the unknown nodal point vectors is obtained by using the submatrices of the global stiffness matrix, K.

The element used most widely for finite element representation is a quadrilateral composed of four triangles having linear velocity distribution [7]. To improve the accuracy of the solution it is desirable to have a complete quadratic velocity distribution throughout the element. This may be accomplished by using a triangular element having three nodal points along each side. However, this is inefficient because the presence of the mid-side nodal points increases the size and bandwidth of the stiffness matrix. This difficulty can be avoided if an incomplete quadratic velocity distribution is introduced for the quadrilateral element such that the velocity along the boundary has a linear variation [8]. Then the velocity distributions take the form of

$$u = \sum_{i=1}^{4} q_i u_i + q_c u_c$$

$$v = \sum_{i=1}^{4} q_i v_i + q_c v_c$$

and

$$q_1 = (1 - s)(1 - t)/4 \qquad q_2 = (1 + s)(1 - t)/4$$

$$q_3 = (1 + s)(1 + t)/4 \qquad q_4 = (1 - s)(1 + t)/4$$

$$q_c = (1 - s^2)(1 - t^2)$$

and u_i and v_i are velocity components at four nodal points for the quadrilateral element; u_c and v_c are those associated with a point within the element (say, the origin of the natural coordinate system); (s, t) represents the natural coordinate system as shown in Fig. 1.

A step-by-step incremental method was employed for the solution of equation (2). The digital computer programs for elastic problems [8] were modified to include the elastoplastic analysis of the present problems. The detailed formulation of the stiffness matrix and the sequence of the computer program are given elsewhere [9].

Results and Discussion

The finite element method not only gives the solution for overall quantities such as load-displacement relationships but also yields detailed information on plastic zone development, stress

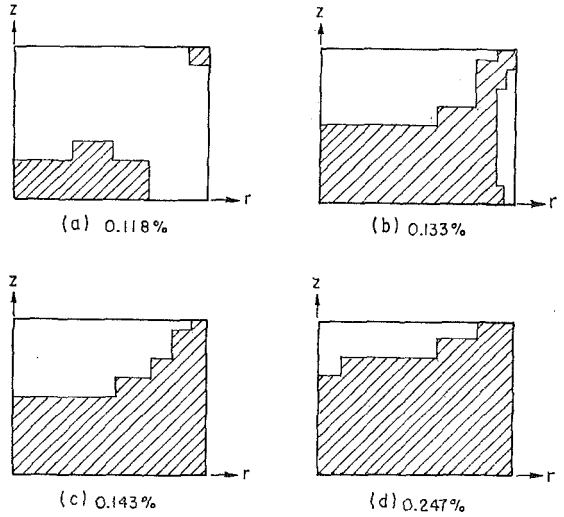

Fig. 3 The plastic zones in axisymmetric upsetting at various reductions in height

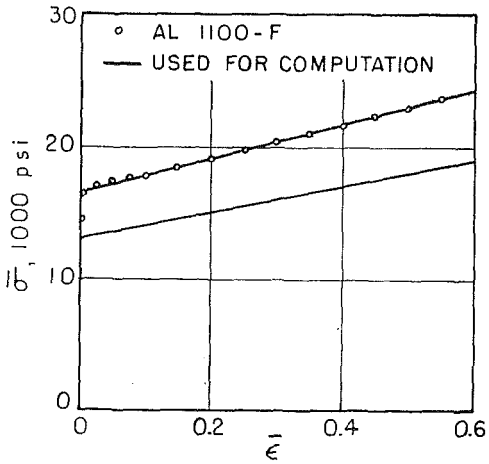

Fig. 4 Stress-strain curves for computer solution of axisymmetric upsetting and stress-strain curves for aluminum 1100-F

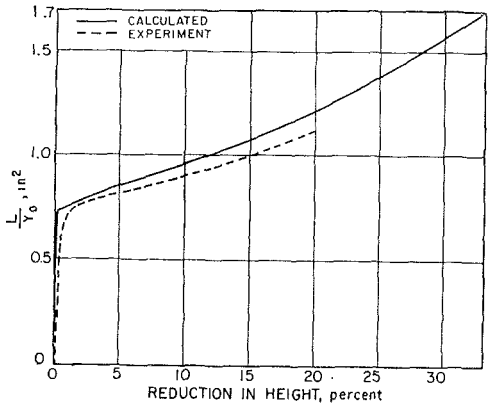

Fig. 5 Computed and experimental load-displacement curves

and strain distributions, and the geometrical change of the free surface. The accuracy of the computed solutions, however, depends on the proper choice of the element shape, the number of elements, and the form of the velocity distribution function assumed within the element. Since the convergence of the computed solutions was not examined in detail, the accuracy of the solution, particularly in the range where the strains are large, is not known. Therefore, the experimental measurements such as the load-displacement curve, free surface profiles, and the hardness distributions were made to evaluate the merit of the computed solutions. It must be noted that material properties should be similar in their flow patterns for a quantitative comparison between the experimental results and the computed solutions. In order to produce similar flows for two strain-hardening metals,

$$(E/Y)_1 = (E/Y)_2$$

and $\bar{\sigma}/Y$ must be the same function of $\bar{\epsilon}^p$ where E is the modulus of elasticity; Y, the initial yield stress; $\bar{\sigma}$, the flow stress; and $\bar{\epsilon}^p$, the plastic effective strain [10]. When a large plastic deformation is involved, the effect of the elastic property can be negligible. The present solutions computed with a specific material property are then applicable to a group of materials with similar plastic properties.

Axisymmetric Upsetting. A cylindrical specimen with a height-diameter ratio of 0.8 was compressed in its axial direction between two flat parallel dies. Since the dies were assumed to be rigid and rough, no relative displacement was permitted at the tool-workpiece interface. The material properties used for the analysis were E (Young's modulus) = 10×10^6 psi, ν (Poisson's ratio) = 0.33, H' (the slope of the effective stress and plastic strain curve) = 20,000 psi, and Y_0 (initial yield stress) = 13,000 psi. The finite element analysis was carried out until a 33 percent reduction in height.

As a preliminary study, two finite element representations were examined, one of 82 elements and the other of 124 elements for half of a cylindrical specimen. The 124 elements were formed with finer divisions along the die contact area, along the free surface, and along two axes of symmetry. Fig. 2 shows the average die pressure and frictional stress as functions of reduction in height. It is evident that the average pressure calculated by the present method is an upper bound and it approaches a better solution as the number of elements is increased. It was also found during this study that a smaller increment of die displacement resulted in a lower value of the average die pressure. Thus, the solution apparently converges to the exact solution as the sizes of both the elements and the displacement increment are reduced. The computed results presented in the following are those based on the 124 elements.

Although our primary concern is the solution in the range of plastic compression, it may be of interest to find how the plastic zone develops from the initial stress-free state. The shapes of plastic zones at some selected reductions are given in Fig. 3. As shown in Fig. 3(*a*), two plastic zones were nucleated, first along the edge of the tool-workpiece interface and then at the center of the specimen. The average die pressure increased linearly with a steep slope. When the plastic zone spread and two zones were connected, as shown in Fig. 3(*b*), the pressure-displacement curve started to bend. The slope of the pressure-displacement curve kept decreasing during the formation of the elastic region of a truncated cone shape beneath the die, Fig. 3(*c*). Then, the sharp bend of the pressure-displacement curve was completed (yield point) and the slope of the curve became approximately constant at the stage shown in Fig. 3(*d*). It must be mentioned that the elastic region beneath the die shrank in size as the compression proceeded and the reduction in height was almost 20 percent when the entire region became plastic. This reduction in height should be compared with the reduction of 0.25 percent at the yield point.

In order to compare actual values with some of the computed results, compression experiments were conducted in which the specimens were prepared from aluminum 1100-F. The initial height of the specimen was 0.75 in. The dies were provided with machined concentric circular grooves to produce a sticking condi-

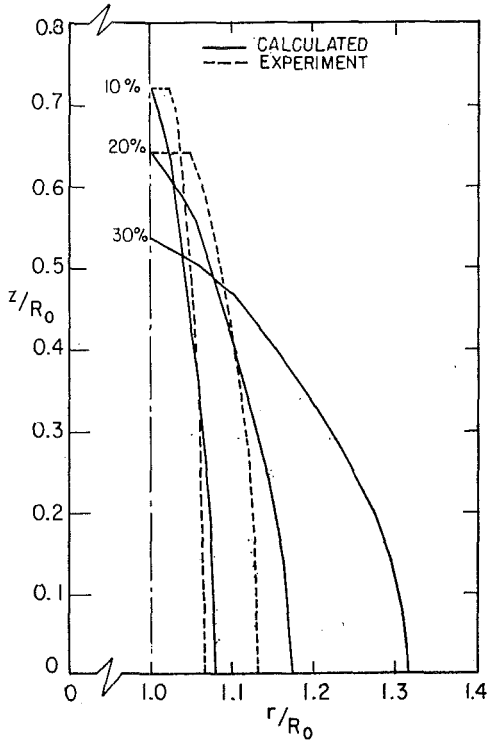

Fig. 6 Theoretical and experimental bulge profiles at various reductions in height

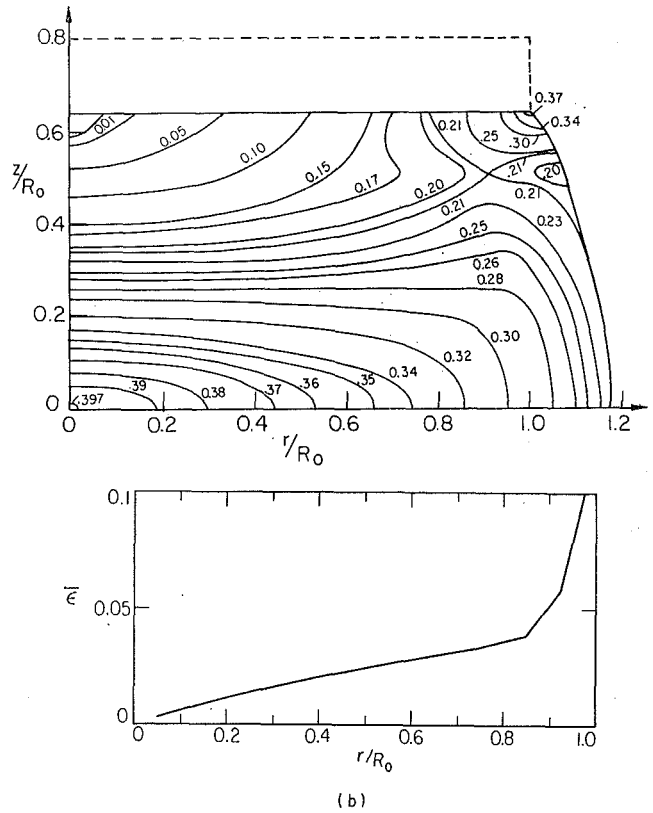

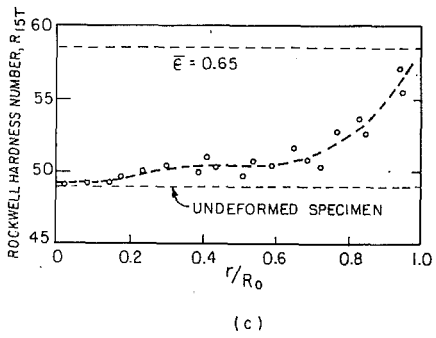

Fig. 7 (a) Computed effective strain distribution at 20 percent reduction in height; (b) computed strain distribution across the contact surface; (c) hardness distribution across the contact surface. Hardness number, R_{15T}, ($^1/_{16}$-in. ball indenter with a 3 kg minor load and a 15 kg major load).

tion at the tool-workpiece interface. The load-displacement curve was recorded, and the bulge profiles of the free surface were measured. Fig. 4 shows the stress-strain property of aluminum 1100-F. The plastic stress-strain relationships of the materials which produce similar flows to those used for computation are also given in the figure. It can be seen that the plastic behavior of aluminum 1100-F is one of the materials to which the computed solution is quantitatively applicable.

The theoretical and experimental load-displacement curves are compared in Fig. 5. Agreement is excellent, with the small deviation attributed to the fact that some differences exist between the theory and experiment with regard to the materials' behavior and the constraint conditions at the tool-workpiece interface.

The finite element method is unique in predicting the geometrical change of the free surface. Fig. 6 shows the bulge profiles at various reductions in height. For small reductions the theory well predicts the geometrical change of the free surface. The predictions, however, deviate more from the observations as the reduction in height increases. It is a well-known fact, as measurements in Fig. 6 indicate, that originally free surface comes into contact with the die at some stage of compression. This phenomenon is more pronounced with increasing frictional constraint at the interface. The results of the finite element analysis did not produce this fact even at a reduction of 33 percent. When originally free surface comes into contact with the die, severe distortion occurs locally, and it appears that much finer elements are required to produce this severe distortion by the finite element method.

The effective strain is an indication of the degree of deformation, and can be calculated by following the deformation at any point incrementally. The computed distribution of the effective strain at a 20 percent reduction in height is shown in Fig. 7. Experimental hardness distribution across the contact surface at the same reduction is also shown for comparison. The distributions of strain components along the axis of the specimen and across the equatorial plane are shown in Figs. 8 and 9, respectively. In Figs. 8 and 9, and also in the subsequent figures, the points in the deformed state are identified by their coordinates in the undeformed geometry. Fig. 8 shows that the axial compressive strain is smallest in its magnitude at the tool-workpiece contact surface and increases toward the center of the specimen. This increase in strain becomes more for a larger reduction in height. The radial and circumferential strains are equal and positive, and the magnitudes are very closely equal to one-half that of the axial strain. Across the equatorial plane, the axial compressive strain is largest at the center and decreases its magnitude toward the free surface. The circumferential strain is larger than the radial strain across the plane except at the center of the specimen.

In simple upsetting, ductile fracture occurs at the barreled surface and the condition of fracture depends on the complete history of the plastic flow. The strain path of the small element on the equatorial free surface was plotted in Fig. 10. Considerable deviation of the path from that for homogeneous deformation

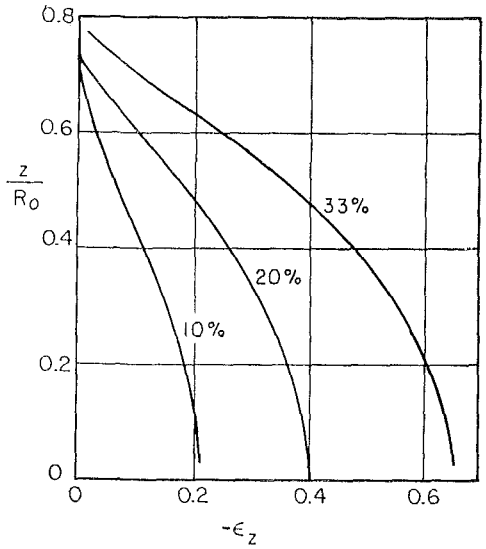

Fig. 8 Axial strain distributions along the axis of the cylinder at various reductions in height

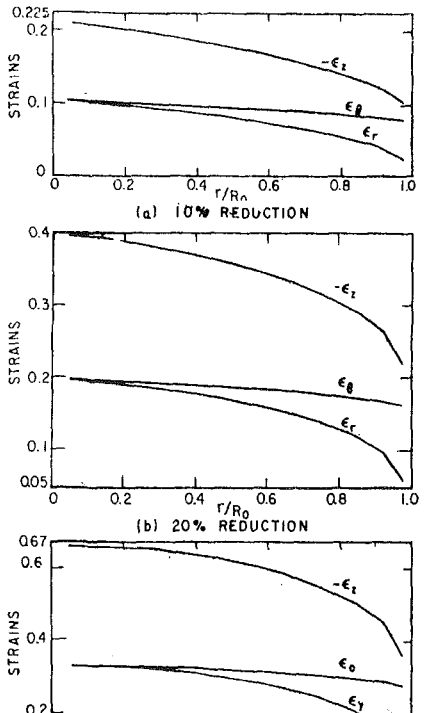

Fig. 9 Distributions of strains across the equatorial plane at various reductions in height

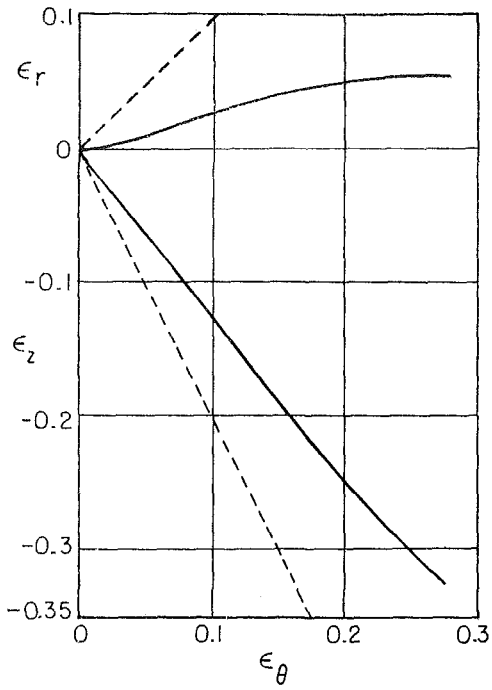

Fig. 10 Strain variations in the element at the equatorial free surface

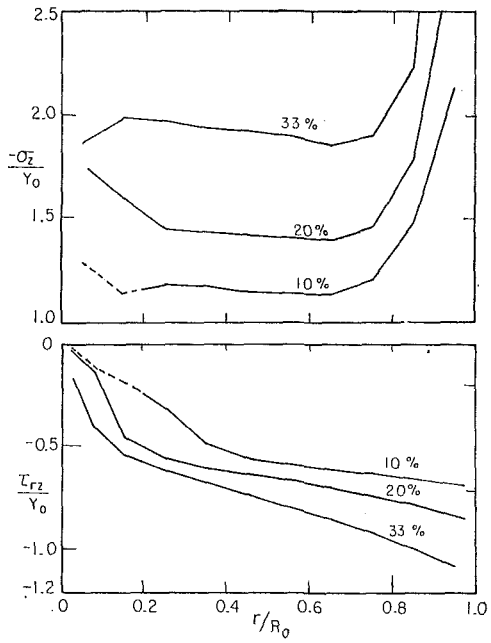

Fig. 11 Distributions of contact pressure and frictional stress at various reductions in height

was apparent since the radial strain increases first and then begins to decrease as the reduction in height increases. These results are in good agreement with the observation made by Kobayashi [11].

Fig. 11 gives the distributions of the normal and shear stresses along the elements in contact with the die at various reductions in height. The contact pressure distribution is more or less uniform over the central area and increases near the edge of the contact surface. A trend showing a slight increase in pressure toward the center appears at a 33 percent reduction. This result indeed coincides with Takahashi's [12, 13] findings in the compression of copper specimens. In his experiments, Takahashi measured contact pressure distribution by the pressure-sensitive pin method for specimens of various height-diameter ratios. He found that in the distributions of contact pressure for specimens with height-diameter ratios larger than unity the largest pressure occurred at the edge of the specimen and the lowest at the center. He also found that the pressure distribution for specimens with height-diameter ratios less than 0.5 showed a friction hill.

The shear stresses are almost zero at the center, and increase

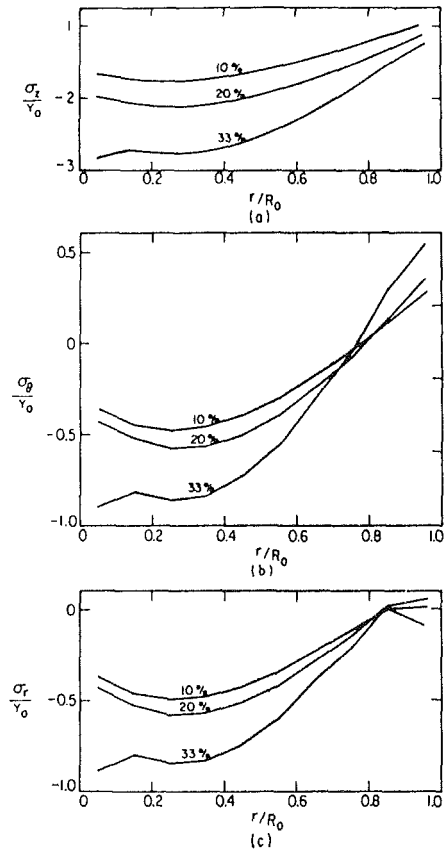

Fig. 12 Distributions of stress components across the equatorial plane at various reductions in height

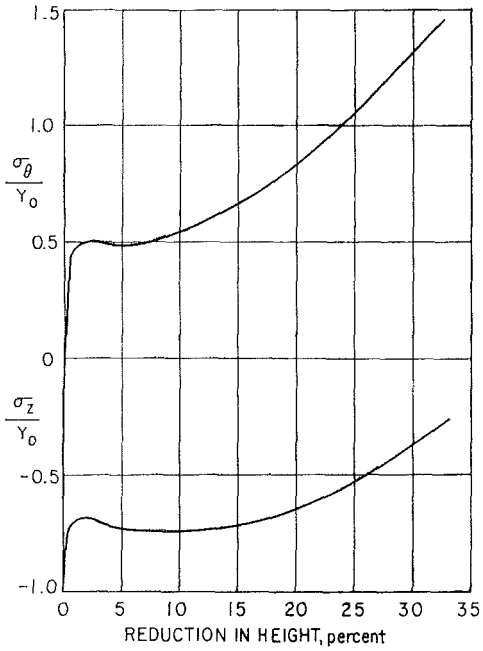

Fig. 13 Variations of stress components at the equatorial free surface as functions of reduction in height

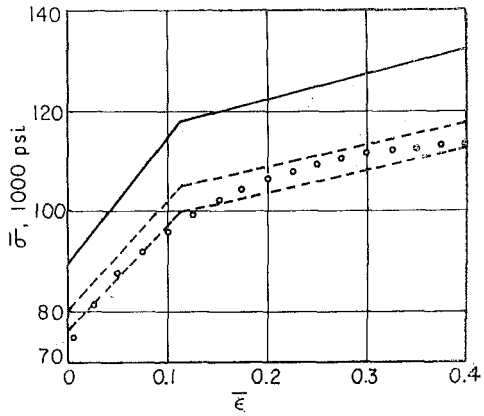

Fig. 14 Stress-strain curves for computer solution of plane-strain side-pressing and for aluminum alloy 7075-T6

first rather sharply and then gradually toward the edge of the specimen. Although the condition of complete sticking used in the computation is an extreme boundary condition, and may never be achieved in reality, the measurements of the interface shear stresses in plastic compression of aluminum disks by Backofen and co-workers [14, 15] confirmed the trend of the computed distribution. In Fig. 12 the stress distributions across the equatorial plane are plotted. The circumferential stress is larger than the radial stress but they become equal near the axis of the specimen. In the central region both stresses are compressive but the circumferential stress becomes tensile while the radial stress approaches zero toward the free surface. The axial stress is compressive and its magnitude decreases from the center to the free surface. The stress variations of the small element on the equatorial surface during compression are shown in Fig. 13. The tensile circumferential stress develops and the compressive axial stress decreases its magnitude as the reduction in height increases. The axial stress may become tensile for still larger reductions. These results are again in agreement with the observations reported in the literature [11, 16].

Plane-Strain Side-Pressing. A cylindrical specimen of initial radius $R_0 = 1/2$ in. was side-pressed between two flat parallel dies under conditions of plane-strain. Complete sticking was assumed at the tool-workpiece interface. An analysis by the finite element method was made in side-pressing up to a reduction in height of 19 percent, using the following material properties:

$$E = 30 \times 10^6 \text{ psi}, \qquad \nu = 0.33$$

$$\bar{\sigma} = Y_0 + H_0'(\bar{\epsilon}^p) \qquad \text{for } 0 \leqq \bar{\epsilon}^p \leqq 0.112$$

$$= Y_1 + H_1'(\bar{\epsilon}^p) \qquad \text{for } 0.112 \leqq \bar{\epsilon}^p$$

with

$$Y_0 = 90{,}000 \text{ psi}, \qquad H_0' = 250{,}000 \text{ psi}$$

and

$$Y_1 = 112{,}400 \text{ psi}, \qquad H_1' = 50{,}000 \text{ psi}$$

This plastic stress-strain curve is shown by a solid line and those for similar materials are given by dashed curves in Fig. 14. The plastic stress-strain behavior of aluminum alloy 7075-T6, also plotted in Fig. 14, is evidently similar to that used for the computation. Therefore, experimental results obtained with aluminum alloy 7075-T6 [17] were quoted for comparison with the computed solution. The finite element representation for a quarter of the circular cross section consists of 155 quadrilateral elements with finer-sized elements along the free surface. The original specimen had a flat cut 0.10 in. wide.

The theoretical and experimental load displacement curves are compared in Fig. 15. The reason that the calculated curve is not smooth is due to the discrete manner in which the tool-workpiece contact area increases as the height of the specimen is reduced. It is seen that the agreement between the theory and experiments is very good. Observed discrepancy can be at-

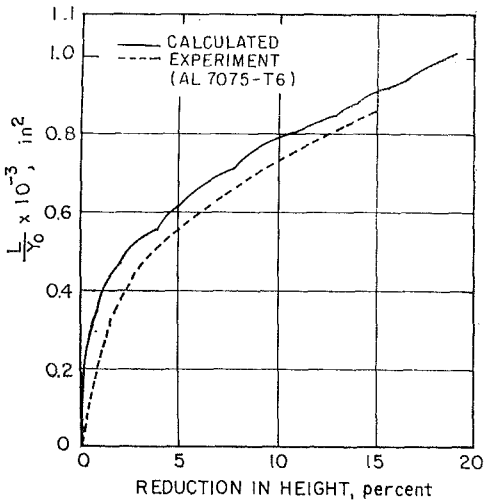

Fig. 15 Computed and experimental load-displacement curves in side-pressing

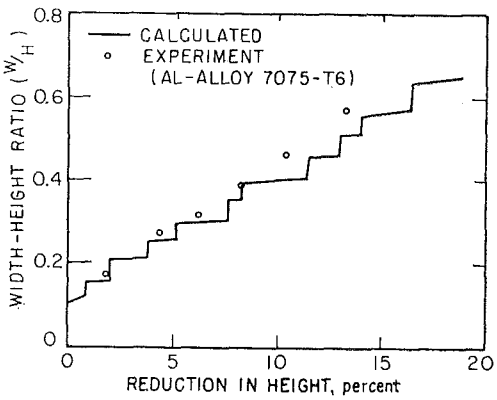

Fig. 16 Contact width-height ratio as a function of reduction in height

tributed to the fact that Young's modulus used in the computation is three times larger than that of aluminum. However, the difference becomes insignificant as the reduction in height increases. The variation of contact-width-height ratio during side-presssing is an important geometrical parameter which dominates the pattern of plastic deformation. The calculated values of width-height ratios are compared with experimental measurements in Fig. 16. The discontinuous variation of calculated width-height ratio is again due to the finite size of the elements along the free surface of the specimen which come in contact with the die as the pressing proceeds. Here, the agreement is excellent, though the initial conditions are slightly different due to an assumed narrow flat cut in the analysis, while the experiment was performed with a circular cylindrical specimen.

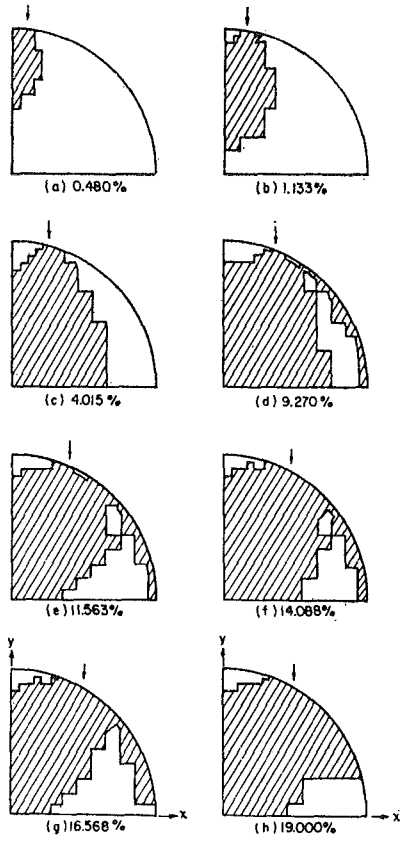

Fig. 17 Plastic zones at various reductions in side-pressing

Unlike axisymmetric upsetting, it is expected from the slip-line theory that during continued pressing some elements may experience unloading. The manner in which the plastic zone develops is not known. It is, therefore, of particular interest to observe the variation of plastic zone size during side-pressing.

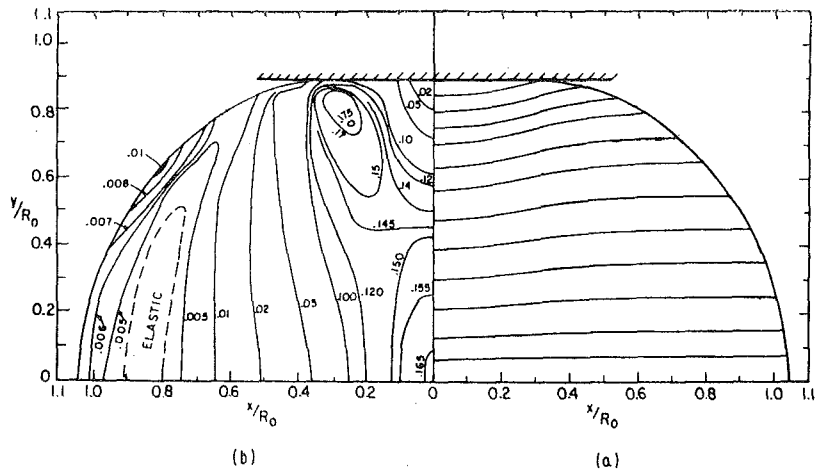

Fig. 18 (a) Line distortions and (b) contours of constant effective strain at 10 percent reduction in height in side-pressing

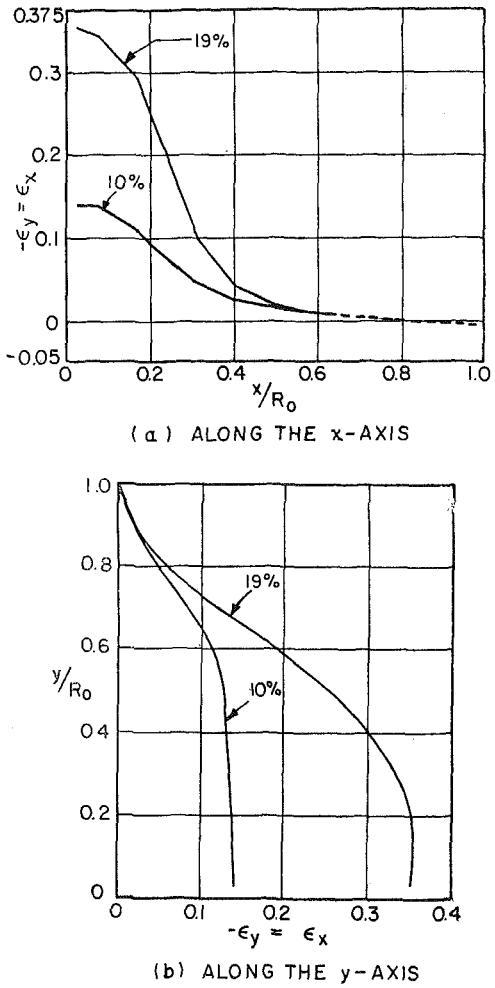

Fig. 19 Strain distributions in the elements along the x and y axes

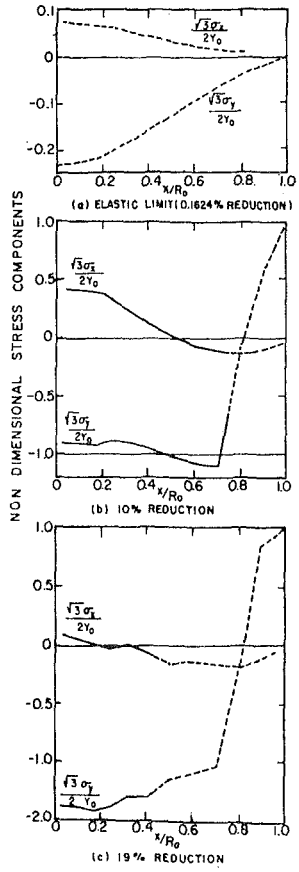

Fig. 20 Stress distributions in the elements along the x axis

The plastic zones at some representative stages are shown in the original geometrical configuration in Fig. 17. The arrows in Fig. 17 indicate the edge of the contact surface. At small reductions, Fig. 17(*a*), the plastic zone development is very similar to that of flat punch indentation [9]. With an increase in reduction in height, the contact width increases and unloading takes place for the elements beneath the die, Fig. 17(*b*). This elastic zone assumes a wedge shape under the die while the plastic zone spreads in the main body, Fig. 17(*c*). As the reduction in height is further increased, the elastic zone beneath the die takes the form of truncated wedge and the elements along the free surface begin to yield, as shown in Fig. 17(*d*). While the size of the elastic zone under the die remains about the same, the size of the elastic zone near the free surface varies in an oscillatory manner for further reductions in height, Figs. 17(*e*), (*f*), (*g*), (*h*). This is caused by the way in which the contact width increases. As soon as a nodal point along a free surface touches the die, the contact width suddenly increases and unloading occurs in some elements. As the die presses, these elements start to deform plastically again until the next surface nodal point comes in contact with the die. At a 19 percent reduction in height, elastic zones are still present beneath the die and near the central free surface.

Fig. 18(*a*) shows distortions of the lines originally parallel to the horizontal axis (*x* axis) at a 10 percent reduction, and the contours of constant effective strain at the same reduction are given in Fig. 18(*b*). The line distortions generally agree with those in the observed pattern. It is of interest to note in Fig. 18(*b*) that relatively large effective strains occurred at the center of the specimen and near the edge of the contact surface. The distributions of the strain components in the elements along the *x* and *y* axes are shown in Fig. 19(*a*) and (*b*), respectively. A large straining can be seen at the center of the specimen and the magnitude of strain decreases rather rapidly toward the central free surface.

The normal stress distributions in the elements along the horizontal axis are shown in Fig. 20. The stress distributions at the elastic limit, given in Fig. 20(*a*), show a marked difference from those at large reductions. It must be noted that the stress distributions at the elastic limit agree very closely with those found in the side-pressing of circular disks using a photoelastic material as the specimen [18]. At large reductions, as seen in Fig. 20(*b*) and (*c*), stress components change their signs near the free surface. The solid parts of the curves represent the elements in the plastic zone and the dashed parts are the stresses in the elastic region. A sharp variation in the stress component σ_y occurred in the elastic region. Fig. 20 clearly indicates that the results obtained by the photoelastic method apply only to small compression, and the stress distributions were quite different when a large deformation occurred.

The stress distributions along the *y* axis are given in Fig. 21. At the elastic limit the compressive stresses are largest at the tool-workpiece contact surface and the magnitudes decrease toward the center of the specimen. The stress component σ_x changes its sign from negative to positive a short distance from the interface, while the stress component σ_y is always compressive. At large reductions in height, the largest compressive stress of the *y* component moved to a distance of approximately one-third the radius of the specimen from the contact surface. Again, the shapes of the stress distributions at large reductions are different from those at the elastic limit. Fig. 22 gives the contact pressure and shear stress distributions. The contact pressure is smallest at the center and increases toward the edge

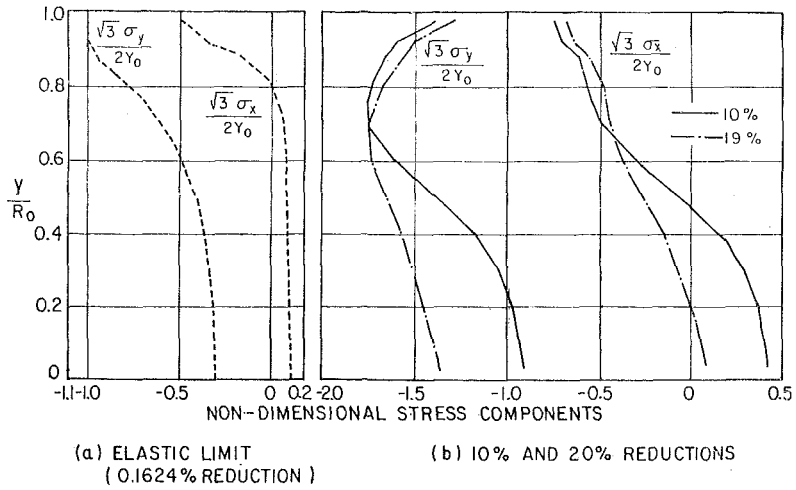

Fig. 21 Stress distributions in the elements along the y axis

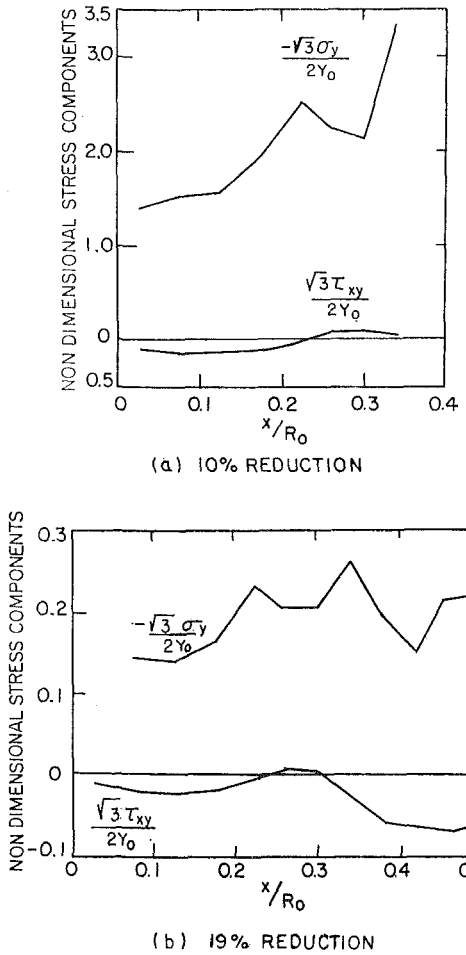

Fig. 22 Distributions of contact stresses at 10 percent and 19 percent reductions in height

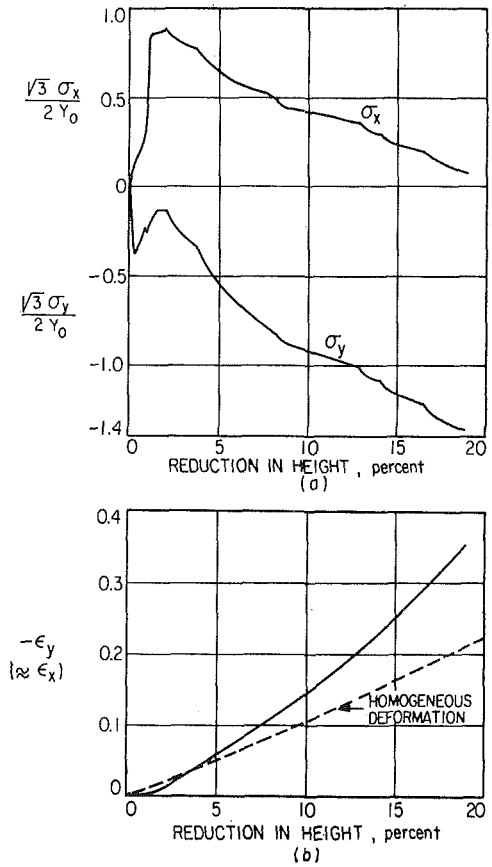

Fig. 23 Stress and strain paths for the element at the center of the specimen in side-pressing

of the contact surface. It is also observed that the contact shear stress is very small. Thus, it can be expected that the effect of the friction condition on the deformation characteristics is negligible. This is indeed the prediction made by the slip-line theory for a rigid perfectly plastic material.

Since the fracture may initiate at the center of the specimen for the present geometrical configuration, it may be of importance to examine the stress and strain paths for the element at the center of the specimen. These are shown in Fig. 23. The stress component σ_x is tensile; it increases at first and then starts to decrease as the reduction in height increases. This variation appears to be attributed to the variation of contact width-height ratio that takes place during pressing, and the effect this has on the deformation pattern.

Concluding Remarks

The finite element method was extended to the analysis of unrestricted plastic flow problems. Since the method permits the following of the deformation from moment to moment, it was

possible to determine the quantities at any instant. The usefulness of the method for detailed studies of deformation characteristics in plastic deformation problems was demonstrated locally and overall in the two selected problems. The plastic zone development, load-displacement curves, geometrical changes of the free surface, and stress and strain distributions were computed and shown to predict well the actual behavior of the material. It was pointed out further that the computed solutions apply quantitatively not only to the specific material used for the analysis but also to a group of materials that produce similar flows. Evidently, the finite element method is a powerful tool for the analysis. However, questions remain with regard to the accuracy of the solutions and the efficiency of the computation. It appears that still another method may be needed for the detailed analysis of plastic deformation processes.

Acknowledgments

The authors wish to thank the National Science Foundation for its grant GK-14946 and the Air Force Materials Laboratory, Wright-Patterson Air Force Base, for its contract AF33615-68-C-1314 under which the present investigation was performed. They also wish to thank the Computer Center, University of California, Berkeley, for the use of computer facilities. They are indebted to Mrs. Naomi Troth for editing the manuscript, Miss LaVerne Marts for typing, and Mr. W. Kot for preparing the figures.

References

1 Zienkiewicz, O. C., and Cheung, Y. K., *The Finite Element Method in Structural and Continuum Mechanics*, McGraw-Hill, London, 1967.

2 Hill, R., "A General Method of Analysis for Metal-Working Processes," *Journal of Mechanics and Physics of Solids*, Vol. 11, 1963, p. 305.

3 Tarnovskii, I. Ya., Pozdeyev, A. A., and Lyashkov, V. B., *Deformation of Metals During Rolling*, Pergamon Press, 1965.

4 Hill, R., *The Mathematical Theory of Plasticity*, Oxford at the Clarendon Press, 1950.

5 Green, A. P., "A Theoretical Investigation of the Compression of a Ductile Material between Smooth Flat Dies," *Philosophical Magazine*, Vol. 42, 1951, p. 900.

6 Bishop, J. F. W., "On the Effect of Friction on Compression and Indentation between Flat Dies," *Journal of the Mechanics and Physics of Solids*, Vol. 6, 1958, p. 132.

7 Wilson, E. L., "A Digital Computer Program for the Analysis of Axisymmetric Solids with Orthotropic Nonlinear Material Properties," Air Force Report No. BSD-TR-67-228, 1967.

8 Doherty, W. P., Wilson, E. L., and Taylor, R. L., "Stress Analysis of Axisymmetric Solids Utilizing Higher-Order Quadrilateral Finite Elements," Report No. S.E.S.M. 69-3, Structural Engineering Laboratory, University of California, Berkeley, Jan. 1969.

9 Lee, C. H., and Kobayashi, Shiro, "Elastoplastic Analysis of Plane-Strain and Axisymmetric Flat Punch Indentation by the Finite Element Method," to be published in the *International Journal Mechanical Sciences*, 1970.

10 Shabaik, A. H., and Kobayashi, Shiro, "Investigation of the Application of Visioplasticity Methods of Analysis to Metal Deformation Processing," Final Report, prepared under Navy, Bureau of Naval Weapons, contract NOw 65-0374-d, Feb. 1966.

11 Kobayashi, Shiro, "Deformation Characteristics and Ductile Fracture of 1040 Steel in Simple Upsetting of Solid Cylinders and Rings," JOURNAL OF ENGINEERING FOR INDUSTRY, TRANS. ASME, Series B, Vol. 92, No. 2, May 1970, pp. 391–399.

12 Takahashi, Soji, "The Distribution of Contact Pressures in Compressing Cylindrical Specimens," *Journal of Japan Society for Technology of Plasticity*, Vol. 6, No. 52, 1965, p. 271.

13 Takahashi, Soji, "Some Experiments on the Contact Pressure Distribution in the Compression of Copper Cylindrical Specimens," *Journal of Japan Society for Technology of Plasticity*, Vol. 9, No. 84, 1968.

14 Van Rooyen, G. T., and Backofen, W. A., "A Study of Interface Friction in Plastic Compression," *International Journal of Mechanical Sciences*, Vol. 1, 1960, p. 1.

15 Pearsall, G. W., and Backofen, W. A., "Frictional Boundary Conditions in Plastic Compression," JOURNAL OF ENGINEERING FOR INDUSTRY, TRANS. ASME, Series B, Vol. 85, No. 1, 1963, p. 68.

16 Kudo, H., and Aoi, K., "Effect of Compression Test Conditions upon Fracturing of a Medium Carbon Steel—Study on Cold-Forgeability Test: Part II," *Journal of Japan Society for Technology of Plasticity*, Vol. 8, 1967, p. 17.

17 Jain, S. C., and Kobayashi, Shiro, "Deformation and Fracture of an Aluminum Alloy in Plane Strain Side-Pressing," presented at the 11th International Conference on Machine Tool Design and Research, Birmingham, England, Sept. 1970.

18 Unksov, E. P., *An Engineering Theory of Plasticity*, Butterworths, London, 1961.